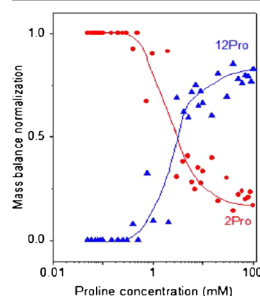


## RESEARCH ARTICLE

# Cooperative Formation of Icosahedral Proline Clusters from Dimers

Alexander D. Jacobs, K. V. Jovan Jose, Rachel Horness, Krishnan Raghavachari, Megan C. Thielges, David E. Clemmer

Department of Chemistry, Indiana University, Bloomington, IN 47405, USA



**Abstract.** Ion mobility spectrometry-mass spectrometry and Fourier transform infrared spectroscopy (FTIR) techniques were combined with quantum chemical calculations to examine the origin of icosahedral clusters of the amino acid proline. When enantiopure proline solutions are electrosprayed (using nanospray) from 100 mM ammonium acetate, only three peaks are observed in the mass spectrum across a concentration range of five orders of magnitude: a monomer  $[\text{Pro}+\text{H}]^+$  species, favored from 0.001 to 0.01 mM proline concentrations; a dimer  $[2\text{Pro}+\text{H}]^+$  species, the most abundant species for proline concentrations above 0.01 mM; and, the dimer and dodecamer  $[12\text{Pro}+2\text{H}]^{2+}$  for 1.0 mM and more concentrated proline solutions. Electro spraying racemic *D/L*-proline solutions from 100 mM ammonium acetate

leads to a monomer at low proline concentrations (0.001 to 0.1 mM), and a dimer at higher concentrations ( $>0.09$  mM), as well as a very small population of 8 to 15 Pro clusters that comprise  $<0.1\%$  of the total ion signals even at the highest proline concentration. Solution FTIR studies show unique features that increase in intensity in the enantiopure proline solutions, consistent with clustering, presumably from the icosahedral geometry in bulk solution. When normalized for the total proline, these results are indicative of a cooperative formation of the enantiopure 12Pro species from 2Pro.

**Keywords:** Proline clusters, Ion mobility spectrometry, Cooperativity

Received: 29 June 2017/Revised: 28 September 2017/Accepted: 1 October 2017/Published Online: 10 November 2017

## Introduction

Electrospray ionization (ESI) [1] of aqueous 0.01 M solutions of the amino acid proline leads to the spontaneous resolution of a proline dodecamer  $[12\text{Pro}+\text{H}]^+$  species that favors a hollow structure, where each proline amino acid is positioned at the vertex of an icosahedron and a single proton is trapped in the interior [2]. This cluster size stands out among a broad distribution of other sizes, extending to nanometer scale assemblies [2–4]. The formation of enantiopure clusters is entropically favored compared with racemic forms [5]. Myung et al. presented an analysis showing that the propensity for 12Pro chiral resolution is even greater than the homochiral preference measured previously for the serine octamer,  $[8\text{Ser}+\text{H}]^+$  [2, 6], a cluster that has captured the imaginations

of many because of its potential as a precursor of biological oligomers (having sequences that are dominated by residues of the same chirality) [7, 8].

In the present paper, we present ion mobility spectrometry-mass spectrometry (IMS-MS), Fourier transform infrared spectroscopy (FTIR), and theoretical quantum chemical studies of proline in aqueous solutions containing 100 mM ammonium acetate. Ammonium acetate buffers the solution to a pH of  $\sim 6.8$ , near the proline isoelectric point ( $pI = 6.3$ ) where proline exists as zwitterion. Remarkably, nano ESI of enantiopure solutions of proline, at concentrations above 1.0 mM, yields only dimers and dodecamers, indicating a cooperative transition between these species. FTIR studies of enantiopure and racemic solutions show differences in vibrational band intensities, and comparisons with theory suggest that these features are consistent with the existence of clusters such as the icosahedral geometry in bulk solution.

The present findings build on a large body of work involving the resolution of specific chiral forms of different amino

**Electronic supplementary material** The online version of this article (<https://doi.org/10.1007/s13361-017-1833-6>) contains supplementary material, which is available to authorized users.

Correspondence to: David Clemmer; e-mail: [Clemmer@Indiana.EDU](mailto:Clemmer@Indiana.EDU)

acids, including: ESI-MS studies of all of the naturally occurring amino acids, a number of unnatural forms [9–15], as well as some spectroscopic studies of the isolated ions [16–19]. Analysis of MS data from mixtures of deuterated and non-deuterated enantiomers have provided direct insight into the magnitude of chiral preferences; interestingly some cluster sizes prefer heterochiral compositions [20–23]. The association of some amino acids is directly relevant to diseases [24]. Others are useful as models for understanding aggregation of larger peptides [25, 26]. Many experiments have focused on issues of chirality that are thought to be possibly associated with the origins of primordial life [27–31]. To this end, studies of the clustering of amino acids on hot surfaces as well as cluster deposition onto surfaces followed by laser and thermal desorption have been conducted [32, 33]. In some cases, amino acids [34–36] and small peptides [37–40] condense to form peptide bonds in unusual environments, leading to oligomers with sequences that incorporate the precursor amino acids [41], as well as unexpected sequences arising from sidechain transformations [42] – providing a fascinating glimpse into the plasticity of amino acid chemistry and the formation of oligomers [8, 14, 41, 42].

## Experimental

### Sample Preparation

Aqueous 100 mM ammonium acetate solutions of *L*-proline and *D*-proline (Sigma-Aldrich, St. Louis, MO, USA) were prepared such that the proline concentration varied by a factor of  $\sim 10^5$ . Racemic solutions were prepared from aliquots of standard solutions containing the different enantiomers. For the FTIR studies, samples were dried to remove all H<sub>2</sub>O and samples were reconstituted in 100 mM ammonium acetate in deuterium oxide (D<sub>2</sub>O) to the desired proline concentrations.

### Ion Mobility Spectrometry-Mass Spectrometry Instrumentation and Measurements

General aspects of IMS theory and instrumentation are described elsewhere [43–53]. Briefly, the IMS-MS experiments described below were performed on a homebuilt 2m drift tube coupled with a time of flight (TOF) mass spectrometer [49, 54, 55]. A schematic presentation of this instrument is shown in Figure 1. Ions are introduced into the gas phase using a commercial nano electrospray source, a Triversa Nanomate (Advion Bioscience, Inc., Ithaca, NY, USA). Ions are stored in a Smith geometry ion funnel and pulsed periodically (150  $\mu$ s) into the drift tube [56]. The drift tube is filled with  $\sim 3.00$  Torr He and is operated under a  $\sim 10$  V $\cdot$ cm<sup>-1</sup> electric field. After mobility separation, ions are transferred into a differentially pumped region and then pulsed into an orthogonal TOF-MS detector. Data are recorded in a nested fashion [46].

### Collision Cross-Section

Drift times ( $t_D$ ) can be converted to collision cross-sections by using the following equation [53]:

$$\Omega = \frac{(18\pi)^{1/2}}{16} \frac{ze}{(k_B T)^{1/2}} \left[ \frac{1}{M_I} + \frac{1}{M_B} \right]^{1/2} \frac{t_D E}{L} \frac{760}{P} \frac{T}{273.2} \frac{1}{N} \quad (1)$$

where  $ze$  is the charge of the ion,  $k_B$  is the Boltzmann constant,  $T$  is the temperature,  $E$  is the electric field,  $L$  is the drift tube length,  $P$  is the pressure, and  $N$  is the neutral number density at STP.  $M_I$  and  $M_B$  are the masses of the ion and the buffer gas, in this case helium.

### FTIR Measurements

FTIR experiments were carried out on an Agilent Cary 670 FTIR spectrometer with a N<sub>2</sub>(l)-cooled MCT detector. Spectra were recorded at 2 cm<sup>-1</sup> resolution. Aliquots of 10  $\mu$ L were placed between CaF<sub>2</sub> windows with a 25  $\mu$ m Teflon spacer. The instrument was purged for 30 min with N<sub>2</sub> prior to data acquisition. The transmission spectrum from the buffer system was used as a reference and subtracted in order to determine the absorption spectrum of the of amino acid solutions.

### Computational Methods and Theory

The location of the electrostatic potential (ESP) minima of the molecule is the likely binding site for an incoming proton. Hence, we have followed a systematic procedure to track the energetically feasible protonated 12Pro clusters. The isomers of [12Pro+H]<sup>+</sup> are constructed by placing the proton near the ESP minima of the parent neutral cluster structure and carrying out geometry optimizations using density functional theory (DFT) (vide infra). The feasible [12Pro+2H]<sup>2+</sup> isomers are then constructed from the parent [12Pro+H]<sup>+</sup> clusters by placing the second proton at the ESP minima in the +1 cluster topography. On energy minimization, the protons in the optimized geometries stay close to the ESP minima (close to the carboxyl oxygen) of the parent cluster. The resulting relative energies of the optimized low-lying cluster isomers included in our analysis fall within an energy window of 0–5 kcal/mol.

The direct calculation of the energies and energy derivatives of 12Pro clusters are computationally expensive. Hence, we have employed the molecules-in-molecules (MIM) fragment-based method [57] for evaluating the energies and energy derivatives for performing structural optimizations and IR spectral simulations. In the MIM fragmentation procedure, we have considered each proline molecule as a separate fragment. Hence, the [12Pro+2H]<sup>2+</sup> cluster is separated into 12 fragments. Subsequently, each fragment interacts with neighboring fragments based on distance and number-based criteria to construct the primary subsystems. The overcounting due to overlapping primary subsystems is taken into account by the inclusion-exclusion principle to yield derivative subsystems. DFT calculations are then carried out on all the subsystems using the same consistent criteria to perform geometry

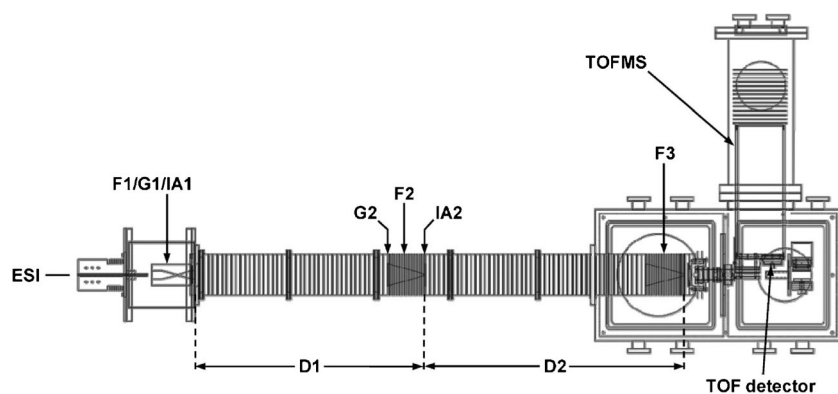


**Figure 1.** Schematic of the homebuilt 2m ion mobility-mass spectrometer

optimizations and IR spectral evaluations on all the  $[12\text{Pro}+2\text{H}]^{2+}$  isomers. Further details on the computational procedure and the method involved in the accurate estimation of the electronic energy, molecular geometry, Hessian matrix, and dipole derivatives through MIM method is discussed elsewhere [57, 58]. MIM fragmentation schemes and IR spectral evaluations are implemented through an external Perl script interfacing the Gaussian 09 program suite [59]. All the optimization and IR frequency evaluations have been done using DFT at the MIM2[MPW1PW91/6-311G(d,p):MPW1PW91/6-31G] level of theory using Gaussian 09. All the located structures are confirmed to be minima on the potential energy surface (PES) with no imaginary frequencies. We have also studied the effects of implicit solvation on the IR spectra of these clusters. For comparing the calculated IR spectra with experiment, we have performed a Boltzmann weighted spectral averaging over the local minima.

## Results and Discussion

### Formation of Proline Monomers, Dimers, and Dodecamers from Ammonium Acetate Solutions

Figure 2 shows representative mass spectra obtained upon electrospraying solutions of  $\sim 10.0$  mM *L*-proline and  $\sim 10.0$  mM *D/L*-proline in 100 mM ammonium acetate. In both spectra, proline dimer,  $[2\text{Pro}+\text{H}]^+$ , is the most abundant species. The only other species detected in the enantiopure solution is the dodecamer,  $[12\text{Pro}+2\text{H}]^{2+}$ . This species is similar to previous work, in which a singly protonated dodecamer was found to be a preferred cluster of proline, favored from enantiopure solutions [2]. The spectrum from the racemic solution shows several low intensity peaks, corresponding to  $[9\text{Pro}+2\text{H}]^{2+}$  to  $[15\text{Pro}+2\text{H}]^{2+}$ , comprising less than 0.1% of the total ion signal, with no enhancement of the  $[12\text{Pro}+2\text{H}]^{2+}$  species. This closely resembles results from previous studies, where aggregation of larger oligomeric species was seen for several charge states [3, 5, 22, 23]. We note that the nanoscale droplets used here do not produce the larger clusters observed previously [2, 3]. Apparently in those studies, many clusters arise as proline associates during the drying of the larger droplets. The total ion count between the two solutions is roughly equal (20,000 for

enantiopure proline and 22,000 for racemic), when the abundance of enantiopure 12Pro is multiplied by six to account for the number of dimers present in the 12Pro species.

Cross-section distributions and new simulated proposed structures for  $[12\text{Pro}+2\text{H}]^{2+}$  are shown in Figure 3 and in Supplementary Figure 1. The measured cross-section for the homochiral  $[12\text{Pro}+2\text{H}]^{2+}$  species is  $286 \text{ \AA}^2$ . When the

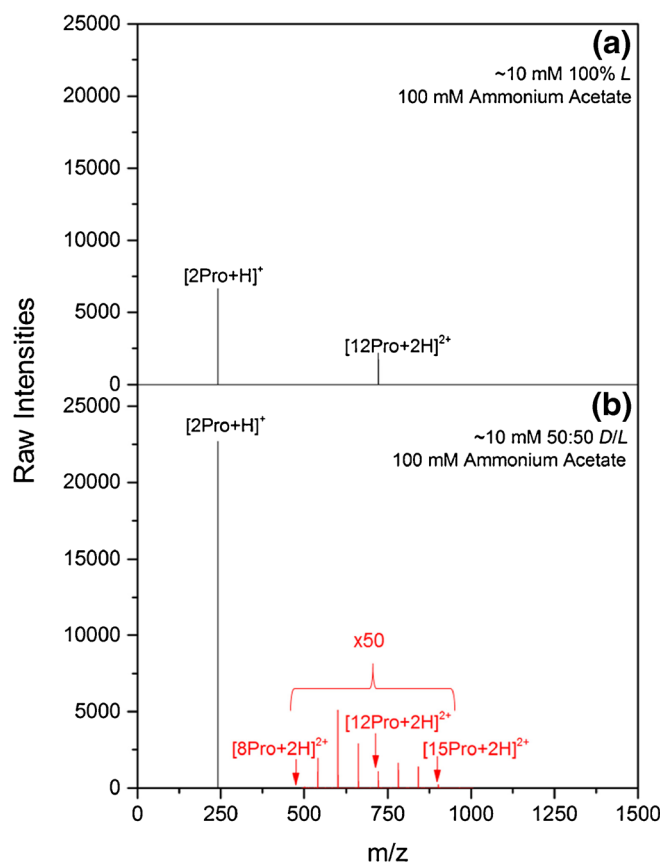


**Figure 2.** Mass spectra of the raw intensities for  $\sim 10$  mM *L*-proline in 100 mM ammonium acetate (a), and  $\sim 10$  mM *D/L*-proline in 100 mM ammonium acetate (b). Low abundance species,  $[9\text{Pro}+2\text{H}]^{2+}$  to  $[15\text{Pro}+2\text{H}]^{2+}$ , from racemic proline are blown up in red. Peaks for  $[8\text{Pro}+2\text{H}]^{2+}$ ,  $[12\text{Pro}+2\text{H}]^{2+}$ , and  $[15\text{Pro}+2\text{H}]^{2+}$  are marked for reference in the racemic solution spectrum, with  $[8\text{Pro}+2\text{H}]^{2+}$  present at higher concentrations

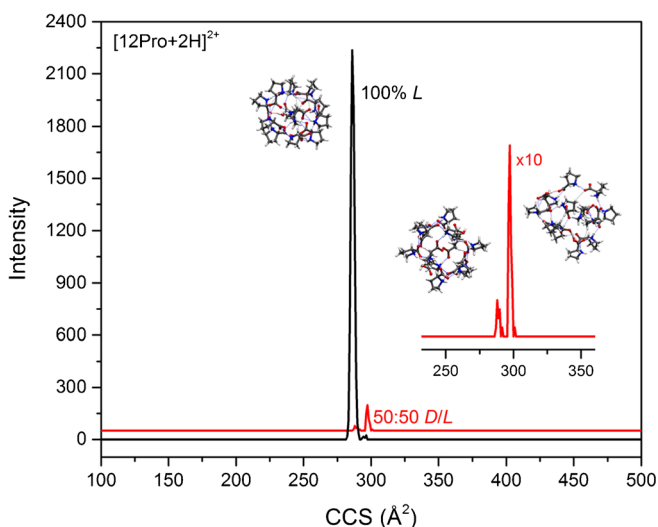


**Figure 3.** Cross-section distributions of  $[12\text{Pro}+2\text{H}]^{2+}$  of *L*-proline (black) and *D/L*-proline (red), with candidate structures superimposed on the distributions. The major peak in *L*-proline consists of an icosahedron, whereas racemic proline has two features, an icosahedron and a twisted icosahedron. The inset shows *D/L*-proline cross-section distribution enlarged to see the two conformations clearly

icosahedron is simulated with two protons instead of one, the calculated cross-section for the new structure shown in Figure 3,  $\Omega = 287 \text{ \AA}^2$ , is in good agreement with the experiment values and is 2% larger than the cross-section,  $\Omega = 281 \text{ \AA}^2$ , reported by Myung et al., for the  $[12\text{Pro}+\text{H}]^+$  species [2]. The larger icosahedron likely arises because Coulombic repulsion from the additional proton causes the hollow structure to expand slightly.

The new simulation also brings refinement to the previous structure. The addition of a proton reduces the number of proton–proline interactions to stabilize the icosahedron. Previously, the proton was shown to interact with four prolines at any given instant [2]. In the doubly charged 12Pro icosahedron, each proton interacts directly with the carboxylic acid groups from two prolines. Candidate structures for racemic  $[12\text{Pro}+2\text{H}]^{2+}$  suggest that the far less favorable heterochiral *6D/6L* form exists as an icosahedron and a twisted icosahedron. The calculated cross-sections for these two candidate theoretical structures,  $287 \text{ \AA}^2$  and  $299 \text{ \AA}^2$ , are in good agreement with the measured cross-sections for racemic *6D/6L*  $[12\text{Pro}+2\text{H}]^{2+}$ ,  $287 \text{ \AA}^2$  and  $297 \text{ \AA}^2$ , respectively. The additional protons associate with the carboxylic acid groups of proline in these structures as well.

### Formation of the Enantiopure 12Pro Cluster is Concentration-Dependent

Figure 4 shows the concentration dependence of the ESI-IMS-MS data for both enantiopure and racemic proline solutions. At the lowest concentration, 0.001 mM, of enantiopure proline, only  $[\text{Pro}+\text{H}]^+$  proline is present. As the concentration is increased to 0.03 mM,  $[2\text{Pro}+\text{H}]^+$  appears and becomes the only species present at 0.05 mM. From 1.0 to 100.0 mM, both  $[2\text{Pro}+\text{H}]^+$  and  $[12\text{Pro}+2\text{H}]^{2+}$  are present in the mass spectra.

It is remarkable that even across this wide range of concentrations, nano ESI produces only  $[2\text{Pro}+\text{H}]^+$  and  $[12\text{Pro}+2\text{H}]^{2+}$ . For the racemic proline solution, dimer is formed at higher concentrations than the enantiopure solution, 0.1 mM compared with 0.03 mM, respectively, and the  $[2\text{Pro}+\text{H}]^+$  becomes the most abundant species at all concentrations above 0.1 mM. A small population (<0.1%) of larger clusters, 8–15Pro, are observed from the racemic solution at concentrations above 0.4 mM. Between 3 and 7 mM proline, there is a sharp increase in the total count of clusters for both proline solutions, indicating a possible ESI-based formation of the clusters. In the normalized and mass balanced plots, however, only the enantiopure 12Pro cluster shows an increase in relative abundance whereas the racemic proline clusters do not, suggesting these clusters are emerging from solution. If the increase was related to the ESI process, the change in cluster abundance would appear in the normalized and mass balanced plots for both enantiopure and racemic proline solutions.

It is interesting to examine the concentration dependence of cluster formation in more detail. Figure 4 shows that as the proline concentration is increased in the enantiopure solution, the abundances of the 2Pro and 12Pro species also increase. However, above 2 mM the 12Pro abundance increases more rapidly than the 2Pro. This can be observed more clearly in the data that are normalized at each concentration. That is, the relative population of 12Pro increases more rapidly than 2Pro and appears to compete with the 2Pro abundance. At our highest concentration, the 12Pro abundance is ~40% of the total, whereas 2Pro comprises ~60%. An additional normalization that accounts for the total number of prolines in each species is also shown in Figure 4. This shows that 12Pro utilizes the bulk of the available proline in the homochiral solution. This analysis shows that abundance of the enantiopure 12Pro cluster is much greater than clusters formed in the heterochiral solutions. That no intermediates are observed is also remarkable, and is indicative of a cooperative two-state  $6(2\text{Pro}) \rightleftharpoons 12\text{Pro}$  transition in the homochiral system.

Total ion count and total monomeric proline are also shown in Figure 4 in the black dashed and red dotted lines, respectively. The total ion count was calculated by adding the ion counts of each species at each concentration. Total monomeric proline was calculated by multiplying the proline species by the number of prolines that form that species. These values were then added together. Results from these calculations show that for the enantiopure proline solution, while the dimer constitutes most of the ion count, most of the available proline is actually incorporated into the dodecamer, shown in the total monomeric proline. This is reflected in the mass balance normalized plot, also in Figure 4.

### FTIR Measurements of *L*-Proline and *D/L*-Proline Solutions

Figure 5 shows FTIR spectra for solutions of enantiopure and racemic proline, at concentrations of 0.01, 0.5, 10, and 100 mM in 100 mM ammonium acetate in  $\text{D}_2\text{O}$ . These concentrations

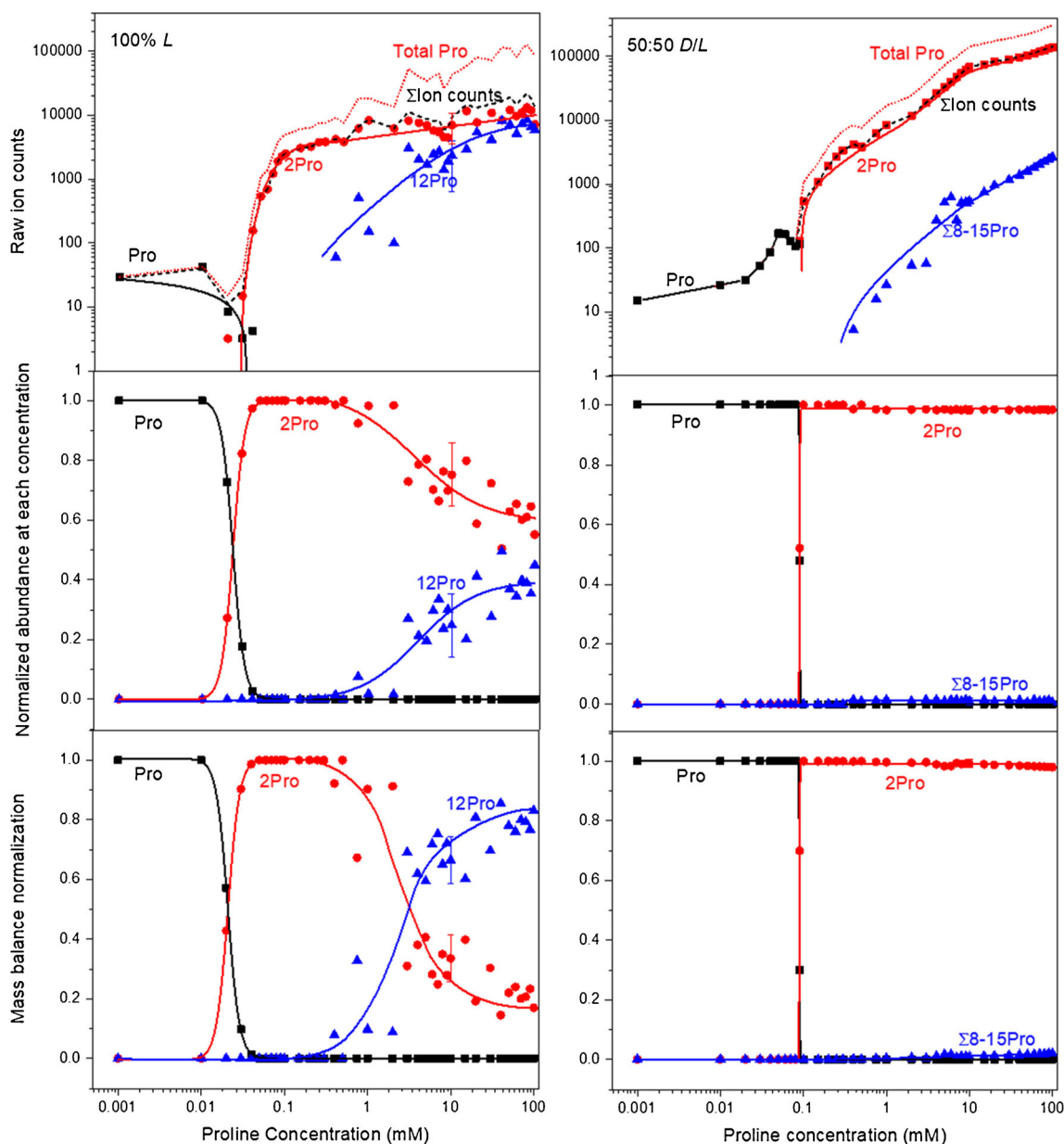


**Figure 4.** Raw ion counts for enantiopure (left) and racemic (right) proline from the ESI-IMS-MS data across a  $\sim 10^5$  concentration range (top), normalized intensity at each concentration across the  $\sim 10^5$  concentration range (middle), and mass balance concentration, which takes into account the total number of prolines in each species (bottom). Black squares represent Pro, red circles 2Pro, blue triangles 12Pro for enantiopure proline and the summation of 8-15Pro for racemic proline, and dashed lines represent the sum of total proline counts (black), and total proline (red). All data are fit with the best fit line to guide the eye. Representative error bars are shown for 10.0 mM. To obtain the mass balanced concentration values, the abundance of a particular species is multiplied by the number of subunits that form that species. Data are then normalized at each concentration

correspond to regions of the MS data where the monomer, dimer, and mixtures of dimer and clusters are observed (see Figure 4). We focus on the IR region between 1000 and 2000  $\text{cm}^{-1}$  because this region leads to the largest differences for the range of solution concentrations. At the lowest concentration of 0.01 mM, at which ESI-IMS-MS predicts the presence of only monomer, there is a broad distribution around 1460  $\text{cm}^{-1}$  that is likely associated with the HOD stretching mode from residual water [60]. As the concentration is increased to 0.5 mM, a sharper feature at  $\sim 1420 \text{ cm}^{-1}$  that is assigned to the  $\text{COO}^-$

symmetric stretch appears for both solutions [61]. At 10.0 mM, the spectra of both enantiopure and racemic proline show additional sharp peaks at  $\sim 1620 \text{ cm}^{-1}$  and  $1560 \text{ cm}^{-1}$  that are ascribed to the  $\text{COO}^-$  asymmetric stretching and the  $\text{NH}_2^+$  scissoring vibration, respectively (Figure 5) [61]. At 100.0 mM, the absorbance of the  $\text{COO}^-$  asymmetric stretch for the enantiopure solution proline shows a dramatic increase. There is more 12Pro present in the ESI-IMS-MS data at this concentration, suggesting that the additional absorbance is related to the presence of larger clusters. We note that the lack of a linear

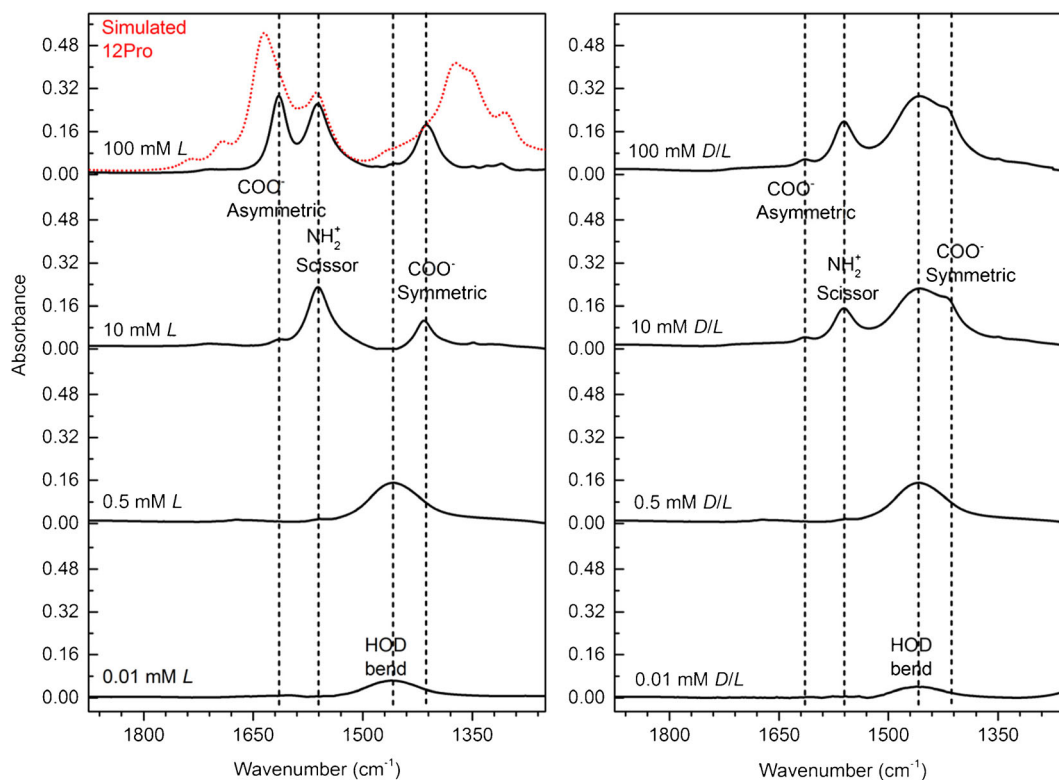


**Figure 5.** FTIR spectra of *L*-proline (left) and *D/L*-proline (right) at concentrations of 0.01, 0.5, 10, and 100 mM. Experimental data is in black solid lines, simulated 12Pro icosahedron is in red dotted lines, shifted down by 5% to account for anharmonicity. Dashed lines and associated labels indicate the vibrations with the greatest changes between the concentrations

response in absorbance at the highest concentrations is likely an outcome of the high concentration used in these studies [62].

Figure 5 also shows a calculated IR spectrum of the theoretical 12Pro structure in solution (scaled down uniformly by 5% to take the anharmonicity into account). Several of the carboxylate stretches are found in the region near the peaks observed for the enantiopure solution, consistent with the presence of clusters. There is far less agreement between the experimental spectrum measured for the racemic proline solution and the calculated 12Pro spectrum. Overall these results require that different species must be present in the racemic and enantiopure bulk solutions. While the results do not unambiguously show that the 12Pro icosahedron is present in the enantiopure solution, these findings are not inconsistent with this conclusion.

## Conclusions

Nano-ESI-IMS-MS experiments have been combined with FTIR measurements and theory to study enantiopure and racemic solutions of proline over a range of concentrations, from 0.001 to 100 mM. The ESI-IMS-MS results show only peaks corresponding to 2Pro and 12Pro for the enantiopure solution at proline concentrations above 1.0 mM. This requires that the 12Pro icosahedron is formed through a cooperative two-state  $6(2\text{Pro}) \rightleftharpoons 12\text{Pro}$  transition. That no intermediates are observed is remarkable. Theoretical calculations are consistent with the

formation of such a structure and when combined with FTIR studies suggest that 12Pro may exist in bulk solution.

## Acknowledgments

K.R. is supported by National Science Foundation [grant number CHE-1665427] at Indiana University. A.D.J. is supported by Robert and Marjorie Mann Fellowship from Indiana University.

## References

1. Fenn, J.B., Mann, M., Meng, C.K., Wong, S.F., Whitehouse, C.M.: Electrospray ionization for mass spectrometry of large biomolecules. *Science*. **246**, 64–71 (1989)
2. Myung, S., Lorton, K.P., Merenbloom, S.I., Fioroni, M., Koeniger, S.L., Julian, R.R., Baik, M.-H., Clemmer, D.E.: Evidence for spontaneous resolution of icosahedral proline. *J. Am. Chem. Soc.* **128**, 15988–15989 (2006)
3. Myung, S., Fioroni, M., Julian, R.R., Koeniger, S.L., Baik, M.-H., Clemmer, D.E.: Chirally directed formation of nanometer-scale proline clusters. *J. Am. Chem. Soc.* **128**, 10833–10839 (2006)
4. Myung, S., Pink, M., Baik, M.-H., Clemmer, D.E.: DL-Proline. *Acta Crystallogr. Sect. C*. **61**, 0506–0508 (2005)
5. Julian, R.R., Myung, S., Clemmer, D.E.: Do homochiral aggregates have an entropic advantage? *J. Phys. Chem. B*. **109**, 440–444 (2005)
6. Julian, R.R., Hodyss, R., Kinnear, B., Jarrold, M.F., Beauchamp, J.L.: Nanocrystalline aggregation of serine detected by electrospray ionization mass spectrometry: origin of the stable homochiral gas-phase serine octamer. *J. Phys. Chem. B*. **106**, 1219–1228 (2002)

7. Takats, Z., Nanita, S.C., Cooks, R.G.: Serine octamer reactions: indicators of prebiotic relevance. *Angew. Chem.* **115**, 3645–3647 (2003)
8. Nanita, S.C., Cooks, R.G.: Serine octamers: cluster formation, reactions, and implications for biomolecule homochirality. *Angew. Chem. Int. Ed.* **45**, 554–569 (2006)
9. Counterman, A.E., Clemmer, D.E.: Magic number clusters of serine in the gas phase. *J. Phys. Chem. B.* **105**, 8092–8096 (2001)
10. Takats, Z., Nanita, S.C., Cooks, R.G., Schlosser, G., Vekey, K.: Amino acid clusters formed by sonic spray ionization. *Anal. Chem.* **75**, 1514–1523 (2003)
11. Nemes, P., Schlosser, G., Vékey, K.: Amino acid cluster formation studied by electrospray ionization mass spectrometry. *J. Mass Spectrom.* **40**, 43–49 (2005)
12. Julian, R.R., Beauchamp, J.L., Goddard, W.A.: Cooperative salt bridge stabilization of gas-phase zwitterions in neutral arginine clusters. *J. Phys. Chem. A.* **106**, 32–34 (2002)
13. Hodyss, R., Julian, R.R., Beauchamp, J.L.: Spontaneous chiral separation in noncovalent molecular clusters. *Chirality.* **13**, 703–706 (2001)
14. Koch, K.J., Gozzo, F.C., Nanita, S.C., Takats, Z., Eberlin, M.N., Cooks, R.G.: Chiral transmission between amino acids: chirally selective amino acid substitution in the serine octamer as a possible step in homochirogenesis. *Angew. Chem. Int. Ed.* **41**, 1721–1724 (2002)
15. Cooks, R.G., Zhang, D., Koch, K.J., Gozzo, F.C., Eberlin, M.N.: Chiroselective self-directed octamerization of serine: implications for homochirogenesis. *Anal. Chem.* **73**, 3646–3655 (2001)
16. Kong, X., Lin, C., Infusini, G., Oh, H.-B., Jiang, H., Breuker, K., Wu, C.-C., Charkin, O.P., Chang, H.-C., McLafferty, F.W.: Numerous isomers of serine octamer ions characterized by infrared photodissociation spectroscopy. *Chemphyschem: Eur. J. Chem. Phys. Physical Chem.* **10**, 2603–2606 (2009)
17. Wyttenbach, T., Bowers, M.T.: Gas-phase conformations: the ion mobility/ion chromatography method. *Top. Curr. Chem.* **225**, 207–232 (2003)
18. Kong, X., Tsai, I.A., Sabu, S., Han, C.-C., Lee, Y.T., Chang, H.-C., Tu, S.-Y., Kung, A.H., Wu, C.-C.: Progressive stabilization of zwitterionic structures in  $[\text{h}(\text{ser})_2\text{-8}]^+$  studied by infrared photodissociation spectroscopy. *Angew. Chem. Int. Ed.* **45**, 4130–4134 (2006)
19. Feketeová, L., Khairallah, G.N., Brunet, C., Lemoine, J., Antoine, R., Dugourd, P., O'hair, R.A.J.: Fragmentation of the tryptophan cluster  $[\text{trp}_9\text{-2h}]^{2+}$  induced by different activation methods. *Rapid Commun. Mass Spectrom.* **24**, 3255–3260 (2010)
20. Julian, R.R., Myung, S., Clemmer, D.E.: Spontaneous anti-resolution in heterochiral clusters of serine. *J. Am. Chem. Soc.* **126**, 4110–4111 (2004)
21. Atlasevich, N., Holliday, A.E., Valentine, S.J., Clemmer, D.E.: Chirality and packing in small proline clusters. *J. Phys. Chem. B.* **116**, 11442–11446 (2012)
22. Atlasevich, N., Holliday, A.E., Valentine, S.J., Clemmer, D.E.: Collisional activation of  $[\text{14pro}+\text{2h}]_2^+$  clusters: chiral dependence of evaporation and fission processes. *J. Phys. Chem. B.* **116**, 7644–7651 (2012)
23. Holliday, A.E., Atlasevich, N., Myung, S., Plasencia, M.D., Valentine, S.J., Clemmer, D.E.: Oscillations of chiral preference in proline clusters. *J. Phys. Chem. A.* **117**, 1035–1041 (2013)
24. Do, T.D., Kincannon, W.M., Bowers, M.T.: Phenylalanine oligomers and fibrils: the mechanism of assembly and the importance of tetramers and counterions. *J. Am. Chem. Soc.* **137**, 10080–10083 (2015)
25. Bleiholder, C., Dupuis, N.F., Bowers, M.T.: Dimerization of chirally mutated enkephalin neurotransmitters: implications for peptide and protein aggregation mechanisms. *J. Phys. Chem. B.* **117**, 1770–1779 (2013)
26. Do, T.D., De Almeida, N.E.C., Lapointe, N.E., Chamas, A., Feinstein, S.C., Bowers, M.T.: Amino acid metaclusters: implications of growth trends on peptide self-assembly and structure. *Anal. Chem.* **88**, 868–876 (2016)
27. Huber, C., Wächtershäuser, G.: Peptides by activation of amino acids with co on (ni,fe)s surfaces: implications for the origin of life. *Science.* **281**, 670–672 (1998)
28. Avalos, M., Babiano, R., Cintas, P., Jimenez, J.L., Palacios, J.C.: Chiral autocatalysis: where stereochemistry meets the origin of life. *Chem. Commun.* **0**, 887–892 (2000)
29. Reiner, H., Plankensteiner, K., Fitz, D., Rode, B.M.: The possible influence of l-histidine on the origin of the first peptides on the primordial earth. *Chem. Biodivers.* **3**, 611–621 (2006)
30. Soai, K., Shibata, T., Morioka, H., Choji, K.: Asymmetric autocatalysis and amplification of enantiomeric excess of a chiral molecule. *Nature.* **378**, 767–768 (1995)
31. Hazen, R.M., Filley, T.R., Goodfriend, G.A.: Selective adsorption of L- and D-amino acids on calcite: implications for biochemical homochirality. *PNAS.* **98**, 5487–5490 (2001)
32. Nanita, S.C., Takats, Z., Cooks, R.G., Myung, S., Clemmer, D.E.: Chiral enrichment of serine via formation, dissociation, and soft-landing of octameric cluster ions. *J. Am. Soc. Mass Spectrom.* **15**, 1360–1365 (2004)
33. Gologan, B., Green, J.R., Alvarez, J., Laskin, J., Graham Cooks, R.: Ion/surface reactions and ion soft-landing. *PCCP.* **7**, 1490–1500 (2005)
34. Rode, B.M., Schwendinger, M.G.: Copper-catalyzed amino acid condensation in water – a simple possible way of prebiotic peptide formation. *Orig. Life Evol. Biosph.* **20**, 401–410 (1990)
35. Chen, F., Yang, D.: Condensation of amino acids to form peptides in aqueous solution induced by the oxidation of sulfur(IV): an oxidative model for prebiotic peptide formation. *Orig. Life Evol. Biosph.* **37**, 47–54 (2007)
36. Ferris, J.P., Hill, A.R., Liu, R., Orgel, L.E.: Synthesis of long prebiotic oligomers on mineral surfaces. *Nature.* **381**, 59–61 (1996)
37. Lee, S., Valentine, S.J., Reilly, J.P., Clemmer, D.E.: Controlled formation of peptide bonds in the gas phase. *J. Am. Chem. Soc.* **133**, 15834–15837 (2011)
38. Lee, S., Julian, R.R., Valentine, S.J., Reilly, J.P., Clemmer, D.E.: Biomolecular condensation via ultraviolet excitation in vacuo. *Int. J. Mass Spectrom.* **316**, 6–11 (2012)
39. Megee, W.M., Mcluckey, S.A.: Efficient and directed peptide bond formation in the gas phase via ion/ion reactions. *Proc. Natl. Acad. Sci.* **111**, 1288–1292 (2014)
40. Shaffer, C.J., Andrikopoulos, P.C., Řezáč, J., Rulišek, L., Tureček, F.: Efficient covalent bond formation in gas-phase peptide-peptide ion complexes with the photoleucine stapler. *J. Am. Soc. Mass Spectrom.* **27**, 633–645 (2016)
41. Yang, P., Xu, R., Nanita, S.C., Cooks, R.G.: Thermal formation of homochiral serine clusters and implications for the origin of homochirality. *J. Am. Chem. Soc.* **128**, 17074–17086 (2006)
42. Takats, Z., Cooks, R.G.: Thermal formation of serine octamer ions. *Chem. Commun.* **0**, 444–445 (2004)
43. St. Louis, R.H., Hill, H.H., Eiceman, G.A.: Ion mobility spectrometry in analytical chemistry. *Crit. Rev. Anal. Chem.* **21**, 321–355 (1990)
44. Hoaglund-Hyzer, C.S., Counterman, A.E., Clemmer, D.E.: Anhydrous protein ions. *Chem. Rev.* **99**, 3037–3080 (1999)
45. Wittmer, D., Chen, Y.H., Luckenbill, B.K., Hill, H.H.: Electrospray ionization ion mobility spectrometry. *Anal. Chem.* **66**, 2348–2355 (1994)
46. Hoaglund, C.S., Valentine, S.J., Spurler, C.R., Reilly, J.P., Clemmer, D.E.: Three-dimensional ion mobility/tofms analysis of electrosprayed biomolecules. *Anal. Chem.* **70**, 2236–2242 (1998)
47. Bluhm, B.K., Gillig, K.J., Russell, D.H.: Development of a fourier-transform ion cyclotron resonance mass spectrometer-ion mobility spectrometer. *Rev. Sci. Instrum.* **71**, 4078–4086 (2000)
48. Hoaglund-Hyzer, C.S., Clemmer, D.E.: Ion trap/ion mobility/quadrupole/time-of-flight mass spectrometry for peptide mixture analysis. *Anal. Chem.* **73**, 177–184 (2001)
49. Koeniger, S.L., Merenbloom, S.I., Valentine, S.J., Jarrold, M.F., Udseth, H.R., Smith, R.D., Clemmer, D.E.: An IMS-IMS analogue of MS-MS. *Anal. Chem.* **78**, 4161–4174 (2006)
50. Mesleh, M.F., Hunter, J.M., Shvartsburg, A.A., Schatz, G.C., Jarrold, M.F.: Structural information from ion mobility measurements: effects of the long-range potential. *J. Phys. Chem.* **100**, 16082–16086 (1996)
51. Wyttenbach, T., Von Helden, G., Batka, J.J., Carlat, D., Bowers, M.T.: Effect of the long-range potential on ion mobility measurements. *J. Am. Soc. Mass Spectrom.* **8**, 275–282 (1997)
52. Wyttenbach, T., Pierson, N.A., Clemmer, D.E., Bowers, M.T.: Ion mobility analysis of molecular dynamics. *Annu. Rev. Phys. Chem.* **65**, 175–196 (2014)
53. Mason, E.A., McDaniel, E.W.: Kinetic theory of mobility and diffusion: Sections 5.1–5.2. Wiley-VCH Verlag GMBH and Co. KGAA., Weinheim (2005)
54. Merenbloom, S.I., Koeniger, S.L., Valentine, S.J., Plasencia, M.D., Clemmer, D.E.: IMS-IMS and IMS-IMS-IMS/MS for separating peptide and protein fragment ions. *Anal. Chem.* **78**, 2802–2809 (2006)
55. Merenbloom, S.I., Koeniger, S.L., Bohrer, B.C., Valentine, S.J., Clemmer, D.E.: Improving the efficiency of ims-ims by a combing technique. *Anal. Chem.* **80**, 1918–1927 (2008)
56. Tang, K., Shvartsburg, A.A., Lee, H.-N., Prior, D.C., Buschbach, M.A., Li, F., Tolmachev, A.V., Anderson, G.A., Smith, R.D.: High-sensitivity

- ion mobility spectrometry/mass spectrometry using electrodynamic ion funnel interfaces. *Anal. Chem.* **77**, 3330–3339 (2005)
57. Mayhall, N.J., Raghavachari, K.: Molecules-in-molecules: an extrapolated fragment-based approach for accurate calculations on large molecules and materials. *J. Chem. Theory Comput.* **7**, 1336–1343 (2011)
58. Jovan Jose, K.V., Raghavachari, K.: Evaluation of energy gradients and infrared vibrational spectra through molecules-in-molecules fragment-based approach. *J. Chem. Theory Comput.* **11**, 950–961 (2015)
59. Frisch, M.J., Trucks, G.W., Schlegel, H.B., Scuseria, G.E., Robb, M.A., Cheeseman, J.R., Scalmani, G., Barone, V., Mennucci, B., Petersson, G.A., Nakatsuji, H., Caricato, M., Li, X., Hratchian, H.P., Izmaylov, A.F., Bloino, J., Zheng, G., Sonnenberg, J.L., Hada, M., Ehara, M., Toyota, K., Fukuda, R., Hasegawa, J., Ishida, M., Naka-Jima, T., Honda, Y., Kitao, O., Nakai, H., Vreven, T., Montgomery, J.A., Peralta, J.E., Ogliaro, F., Bearpark, M., Heyd, J.J., Brothers, E., Kudin, K.N., Staroverov, V.N., Kobayashi, R., Normand, J., Raghavachari, K., Rendell, A., Burant, J.C., Iyengar, S.S., Tomasi, J., Cossi, M., Rega, N., Millam, J.M., Klene, M., Knox, J.E., Cross, J.B., Bakken, V., Adamo, C., Jaramillo, J., Gomperts, R., Stratmann, R.E., Yazyev, O., Austin, A.J., Cammi, R., Pomelli, C., Ochterski, J.W., Martin, R.L., Morokuma, K., Zakrzewski, V.G., Voth, G.A., Salvador, P., Dannenberg, J.J., Dapprich, S., Daniels, A.D., Farkas, Å., Foresman, J.B., Ortiz, J.V., Cioslowski, J., Fox, D.J.: *Gaussian 09*, Rev d.01. Gaussian Inc., Wallingford (2009)
60. Lappi, S.E., Smith, B., Franzen, S.: Infrared spectra of h(2)16o, h(2)18o, and d(2)o in the liquid phase by single-pass attenuated total internal reflection spectroscopy. *Spectrochim. Acta A Mol. Biomol. Spectrosc.* **60**, 2611–2619 (2004)
61. Herlinger, A.W., Long, T.V.: Laser-raman and infrared spectra of amino acids and their metal complexes. iii. proline and bisprolinato complexes. *J. Am. Chem. Soc.* **92**, 6481–6486 (1970)
62. Robinson, D.Z.: Quantitative analysis with infrared spectrophotometers. *Anal. Chem.* **23**, 273–277 (1951)